Thermochimica Acta, 231 (1994) 87–108
Elsevier Science B.V., Amsterdam
SSDI 0040-6031(93)01340-9

High-accuracy thermal analysis of the solid–solid phase transition of lithium sulfate powders

Moisés Tischler

Instituto Nacional de Tecnología Industrial, C.C. 157–1650, San Martín (Argentina)

(Received 3 March 1993; accepted 28 April 1993)

Abstract

Powder samples of Li_2SO_4 from three different manufactures were analysed using an accurate high-resolution heat flow calorimeter. It is shown that some of the results presented are endowed with more than ten times smaller uncertainty limits than are usually encountered in the technical literature covering the state of the art of thermal analysis. Details of the measuring system are given, and reasons for the higher accuracy are discussed.

The average enthalpy change associated with the transformation between the two high temperature forms of solid lithium sulfate, resulted in $\Delta H = 26.1 \pm 1.7$ kJ mol^{-1}. The relatively large uncertainty (twice as large as expected from the calorimeter's performance) is due to unexplained differences between the three powder samples investigated.

Different transformation temperatures were determined for each one of the samples. The origin of the differences, as well as the shape of the measured heat-flow curves, can be explained semi-quantitatively by means of the Gibbs–Thomson effect, in terms of the size distribution of the crystallites that compose the sample, which should depend on its initial granulometry and the dehydration procedure used.

The onset temperatures for the monoclinic to cubic transformation, for sample 1 (Aldrich), sample 2 (Merck), and sample 3 (Alfa), are 577.82 ± 0.08, 577.98 ± 0.05 and 578.30 ± 0.03°C, respectively. They are believed to represent the transformation temperature of the smallest crystallites present in the sample. Extrapolated temperatures, representative of the transformation temperature corresponding to the average crystallite size in samples 1, 2 and 3, are 578.17 ± 0.04, 578.28 ± 0.03 and 578.38 ± 0.02°C, respectively. For the cubic to monoclinic transformation, the corresponding onset temperatures for the same three samples, are 577.90 ± 0.02, 577.84 ± 0.02 and 577.78 ± 0.02°C. These are believed to represent the end temperatures of undercooling, just as nucleation of the new phase begins.

Interphase curvature is such that the monoclinic phase is on the concave side of the interphase.

INTRODUCTION

High accuracy, two of the key words in the heading of this paper deserve clarification right from the very beginning. It will be shown that some of the results presented here are endowed with more than ten times smaller uncertainty limits than are usually encountered in the technical literature

covering the state of the art of thermal analysis. It should come as no surprise that such an improvement crystallized in a laboratory dedicated to fundamental thermometry, since a large part of the techniques and instrumentation tricks used in thermal analysis rest upon accurate temperature measurements. Furthermore, we have been searching over the last decade for alternative ways of implementing the International Temperature Scale, looking for procedures and instrumentation that would fit more properly the conditions of our relatively humble laboratory. The end result was the development of Miniature Thermometric Fixed Points, the Thermoelectric Fixed Point Thermometer, and calibration techniques that resemble very closely those of thermal analysis [1–3], taking full advantage of the availability of inexpensive computer control and automatic data reduction.

Lithium sulfate is a material that has received quite a bit of attention in recent years. It is an ionic salt, presenting a reversible solid–solid phase transition (monoclinc $\rightleftarrows$ FCC) at a relatively high temperature ($\approx$578°C) where the stability and accuracy of sensitive platinum resistance thermometers (PRT) begin to call for special care. The high temperature form of lithium sulfate is a plastic (rotator) phase, presenting an unusually high ionic conductivity, deserving therefore the name of solid electrolyte [4, 5]. From the practical point of view its importance may rest on its application as an electrolyte for high-energy batteries, or as a stable nontoxic material for thermal energy storage [6], since the reversible solid–solid transition involves a large enthalpy change, or as a standard reference material for calibrating thermal-analysis equipment [7].

From the theoretical point of view, the rather tight packing of the Li and the SO_4 ions in the f.c.c.-cell, has led several authors to interesting considerations in order to explain the ability of the Li ions to migrate from one crystal site to the next under the influence of an applied electric field. High-frequency rotations of otherwise stationary sulfate groups, synchronized between neighbors, and tuned with Li-ion jumps (paddle wheel mechanism) [8], as opposed to diffusion mechanisms (percolation) have been invoked, and still are the subject of many recent papers defending one or the other point of view [9]. For all these reasons lithium sulfate seemed to be an appropriate material to investigate, testing at the same time the capabilities of our heat flow calorimeter.

EXPERIMENTAL

Samples

Several powder samples of Li_2SO_4 were analysed using an accurate high-resolution heat flow calorimeter. The powders used were from three different manufacturers. Figures 1(a), 1(b), and 1(c) are electron-micrographs

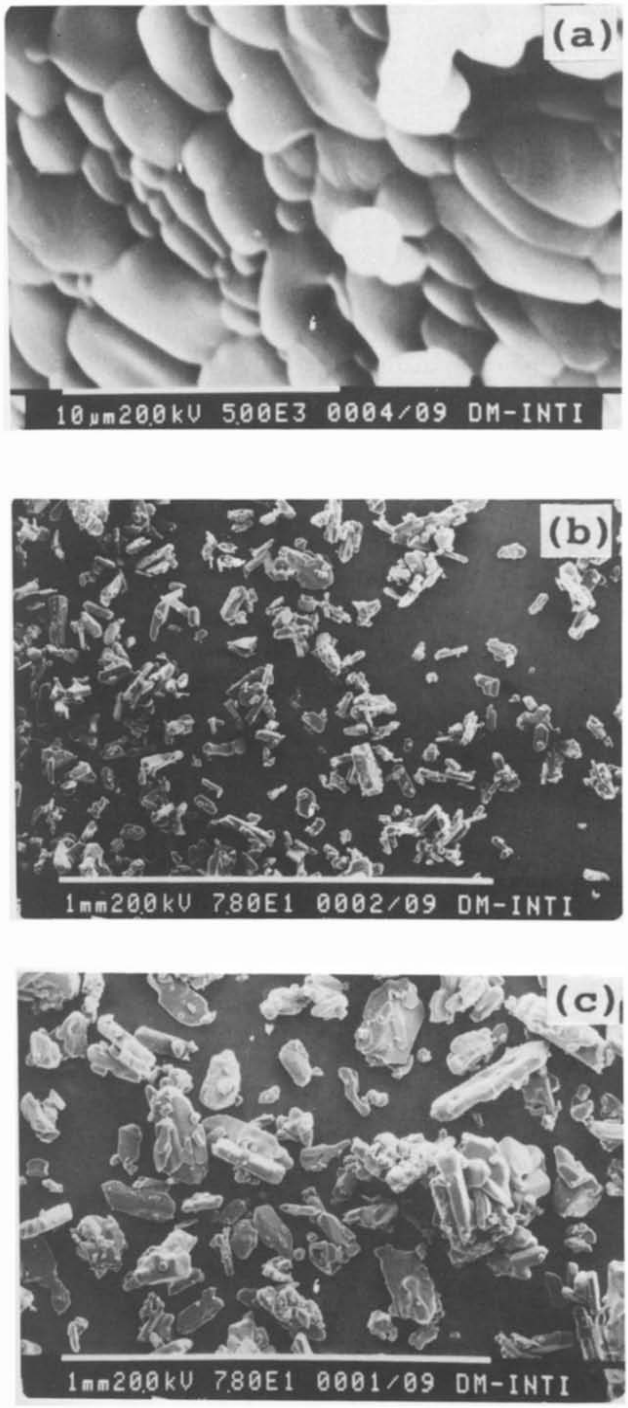

Fig. 1. Electron micrographs of the three samples investigated, as received: (a) Aldrich, (b) Merck, (c) Alfa. Scale: the white horizontal bar represents 10 μm in the first case, and 1 mm in the other two cases.

of samples 1, 2 and 3 respectively, and represent the samples as originally received. Sample 1 (Li_2SO_4, Aldrich Chemical Company, Inc., purity >99.99%) consisted of irregular clusters of small particles. The clusters had typical lengths ranging from 10 μm through 300 μm, but each cluster consisted of crystallites with typical lengths between 0.5 and 15 μm. Sample 2 ($Li_2SO_4 \cdot H_2O$, E. Merck, Darmstadt, Suprapur) consisted of irregular crystallites with typical lengths between 5 and 150 μm. The typical lengths of the crystallites in sample 3 ($Li_2SO_4 \cdot H_2O$, Alfa Products, Ultrapure) ranged from 15 to 400 μm.

In every case the powder samples (≈20 mg) were packed into spectrographic pure graphite capsules and dehydrated. The dehydration process consisted of placing the graphite capsules in a vacuum furnace, which was initially full with air at room temperature. After about 2 h of slow heating and pumping, the sample attained 150°C under a vacuum of 0.3 Pa. It was kept under these conditions 2 h longer, in order to ensure full dehydration. The dehydration was checked by weighing first the empty graphite capsules, then after filling with the hydrated lithium sulfate, and finally immediately after dehydrating. The filled graphite capsules were placed immediately into the calorimeter's sample holder and kept at a temperature close to the solid–solid phase transition under study (≈578°C).

Many measurements, involving repeated transformations from the monoclinic into the cubic phases, and vice versa, were performed over periods of several days, without cooling the sample by more than 2°C. No significant differences in the enthalpy changes or in the transition temperatures, to be reported below, could be determined between one run or the next. This indicates that the sample preparation procedure left a thermally stable product, in every possible sense (dehydration products, impurities, interaction with the graphite capsule, etc.).

In order to gain some insight into the possible effects of dehydration, the samples as shown in Fig. 1 were heated in air for about 0.5 h, and observed again with the electron microscope. The somewhat large crystallites in samples 2 and 3 presented star-like cracks radiating from a common center, and a very porous appearance. Sample 1, although presenting also a few such cracks, seemed less affected.

Sample holder

The graphite capsules are cylindrical, of 3 mm outer diameter and 10 mm long (see Fig. 2). The inner volume containing the sample is of 2 mm diameter and 7 mm long, and is accessible by removing a graphite lid that fits tightly. The calorimeter's sample holder is a cylindrical platinum capsule of 0.2 mm wall thickness, and about 3 mm inner diameter into which the graphite capsules, containing the powder sample, fit snugly.

The two legs of a Pt–10%Rh/Pt thermocouple are welded on opposite sides of the platinum capsule so that the thermoelectric circuit closes

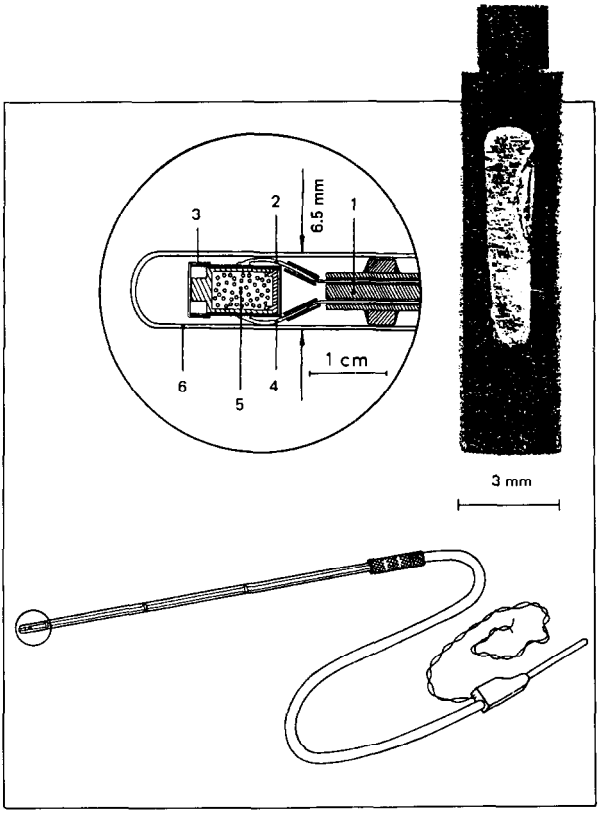

Fig. 2. The thermoelectric fixed-point thermometer, also used as sample holder for thermal analysis: 1, twin bore alumina insulator; 2 and 4, thermocouple legs; 3, platinum capsule with removable lid; 5, miniature thermometric fixed-point, or graphite sample holder, and a photograph of its cross-section; 6, closed-end sanded fused-quartz protection sheath.

through the sample holder. The thermoelectric signal generated by the thermocouple measures the capsule temperature, T_{cap}. In fact, the sample holder and the thermocouple constitute an independent thermometer (Thermoelectric Fixed Point Thermometer) whose details are also shown in Fig. 2 [2,3]. Its cold junction is kept in an ice bath whose temperature differs from 0°C by less than ±1 mK.

Calorimeter

The calorimeter (Fig. 3) consists of a quasi-isothermal volume (hereafter referred to as environment) with a typical length of about 100 mm and temperature gradients of less than 10 mK, whose temperature is T_{env}. The latter is measured with a high precision platinum resistance thermometer (PRT) immersed in the environment, of the type used to implement the International Temperature Scale of 1990 (ITS-90) [10]. The sample holder,

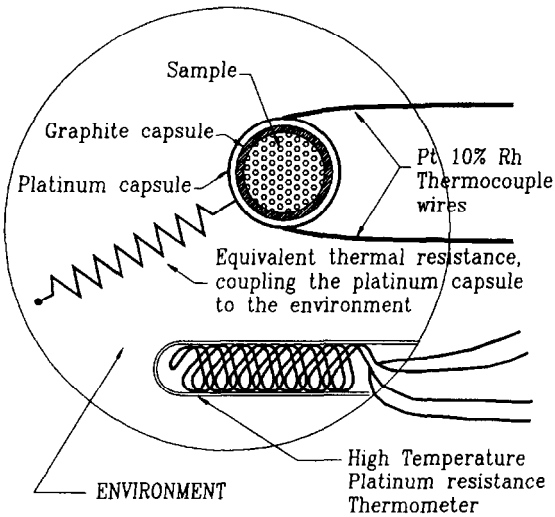

Fig. 3. Schematic representation of the calorimeter: the outer circle represents the quasi-isothermal environment whose temperature, T_{env}, is measured with the precision platinum resistance thermometer, calibrated according to ITS-90.

placed alongside the PRT, can be envisioned as thermally coupled to the isothermal volume through an effective thermal resistance R, over which all heat exchanges with the environment take place.

The temperature T_{env} can be varied with a rate, β, as low as 1 mK min^{-1} under control of a personal computer (PC) which acquires at the same time all the relevant data (T_{env}, T_{cap}, time, etc.).

The accuracy with which these measurements can be made is mainly limited by the fact that a thermometer measures its own average temperature, which is not necessarily the temperature that one is looking for. The degree to which the indicated temperature is the same as the thermodynamic temperature of the sample, depends upon

(a) the nature of the thermal contact between thermometer and sample, i.e. thermal resistance to heat flow between their different parts;

(b) the heating rate β, in relation to the heat capacities of the thermometers, the sample, and all the parts making up the environment;

(c) the steady state temperature distribution around and over the sample and the thermometers;

(d) calibration of the thermometers and traceability to the ITS-90.

Ideally, in the limiting case $\beta = 0$, the environment's, sample's, and thermometer's temperature are the same, since transient temperature gradients are thereby minimised. However even then, undetected steady-state temperature gradients may be present, so that the temperature indicated by the thermometers might differ from that of the sample. Moreover different parts of the sample might be at different temperatures.

Thermodynamic equilibrium is also of main concern for accurate thermal

analysis. This requires very slow heating rates with typical times much larger than any relaxation time that the sample might require for thermal and atomic diffusion to take place. Also interphase energies related to surface tension, usually neglected, may be relevant when phase equilibria are investigated. Its importance in the case of powder samples will become apparent below.

The measuring system used for the present study of lithium sulfate (to be fully described elsewhere), minimises some of these systematic sources of error. The low temperature gradients in the environment (<10 mK) are achieved using a computer controllable three-zone furnace equipped with a heat pipe [11]. ITS-90 thermometric calibration of the PRT using miniature thermometric fixed points [3] and its "in situ" transfer to the sample-holder's thermocouple during each experiment ensure T_{env} and T_{cap} measurements accurate to better than ±10 mK. Controllable heating rates of as low as 1 mK min^{-1} ensure a homogeneous temperature distribution and a high degree of thermodynamic equilibrium. Even heating rates as large as ±40 mK min^{-1} have empirically proven that while the sample does not undergo any phase change, the average value of the difference $|(T_{env} - T_{cap})|$ is smaller than 1.5 mK, with a standard deviation around the average of ±3 mK. This indicates that heat capacity effects (i.e. thermal lag of the thermometers, including sample holder and sample) are entirely negligible for such (or lower) heating rates.

The thermal resistance R (see Fig. 3) is determined by the constructive details of the calorimeter, i.e. geometry and materials, which are obviously held fixed, as well as by the temperature T_{env}. The functional dependence, $R(T_{env})$, can be determined empirically using standard materials of known latent heat of transformation. Figure 4 represents $R(T_{env})$ versus T_{env},

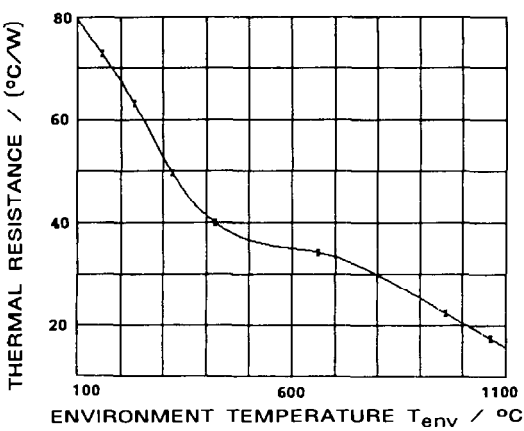

Fig. 4. Calibration curve of the calorimeter: equivalent thermal resistance vs. environment temperature. The crosses represent the calibration points (In, Sn, Cd, Zn, Al, Ag, Au). The continuous curve represents a cubic spline interpolation.

determined using the melting points of In, Sn, Cd, Zn, Al, Ag and Au. Interpolation between these calibration points, in order to calculate the thermal resistance at any desired temperature, is performed using cubic splines. The accuracy of the whole procedure is better than ±3%, as was determined by removing one of the calibration points at a time, and treating it as an unknown material whose enthalpy change is under investigation. For that purpose the interpolation procedure was also varied using linear, parabolic and cubic splines. This numerical procedure for testing self consistency, indicates also that the latent heats of the metals used as reference standards, as taken from the literature [12], are accurate at least within the uncertainty limit mentioned above (not one of the results

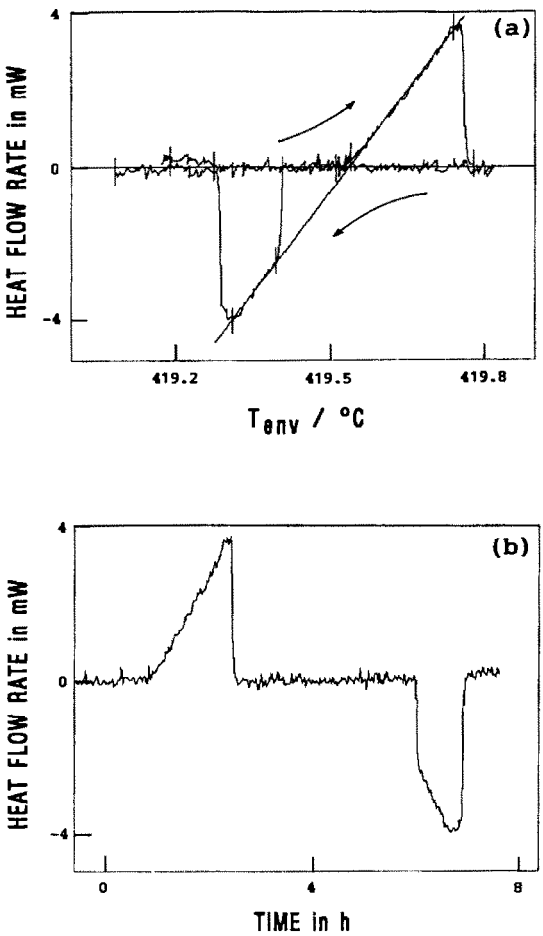

Fig. 5. Measured curves for melting and freezing Zn. (a) Heat flow rate vs. environment temperature, the arrows indicate increasing time. Notice the sudden jump on the negative heat flow rate side, corresponding to undercooling. (b) Heat flow rate vs. time.

differed from the expected value by more than ±3%). The value of R(578°C) for lithium sulfate resulted in $(35.2 \pm 1)\ \mathrm{K\ W^{-1}}$.

The heat flow rate into the sample is given by $\phi = (T_{env} - T_{cap})/R(T_{env})$, an expression that is essentially the definition of $R(T_{env})$. A typical experiment performed with this calorimeter is illustrated in Fig. 5, for the case of the melting and freezing of about 100 mg of Zn, with a nominal purity of 99.9999%. Figure 5(a) represents the heat flow rate into the sample as a function of T_{env}. The positive portion corresponds to heating (increasing T_{env}, $\beta = 2.5\ \mathrm{mK\ min^{-1}}$) while the negative portion corresponds to cooling (decreasing T_{env}, $\beta = -2.5\ \mathrm{mK\ min^{-1}}$). The intersection between the two line segments determines the phase transition temperatures of the sample, which in this case differs from the ITS-90 value by less than 5 mK. The same figure shows also that the Zn sample undercooled 0.14 K before the solid phase appeared. Figure 5(b) corresponds to the same experiment and represents the heat flow rate as a function of time. The area under the first peak is the latent heat of melting, while the area under the second peak is the latent heat of freezing. In fact, considering the Zn sample as a reference material, the value of the corresponding thermal resistance at the Zn point $R(419.527°C) = (40 \pm 0.5)\ \mathrm{K\ W^{-1}}$ was calculated from this experiment, and constitutes one of the calibration points that led to the curve illustrated in Fig. 4. The same experiment is also used for the ITS-90 calibration of PRTs at the Zn point.

RESULTS FOR LITHIUM SULFATE

Figures 6–8 represent typical curves for the three samples of Li_2SO_4 investigated. They correspond to runs during which the complete sample, initially in the monoclinic form, was converted into the cubic form (positive heat flow rate), or runs during which the complete sample, initially in the cubic form, was converted into the monoclinic form (negative heat flow rate). Other experiments, to be discussed below, were such that after converting only part of the sample from the monoclinic into the cubic form, the heating rate was reversed (it became a cooling rate) in order to reconvert the material to its initial form.

The average heating or cooling rates, β, used for these experiments were between 8 and 20 $\mathrm{mK\ min^{-1}}$. The time that it took to transform a 20 mg sample from one phase to the other varied accordingly from about 60 to about 30 min.

The analysis of the curves consisted of determining the onset temperature, T_i, and the extrapolated temperature, T_e (see for example Fig. 8(a)). The former is the temperature at which the absolute value of the heat flow rate begins to increase from a value which is low enough to be buried in the noise of the baseline (the line corresponding to $\phi = 0$). The extrapolated temperature, T_e, is determined by the intersection between the tangent at

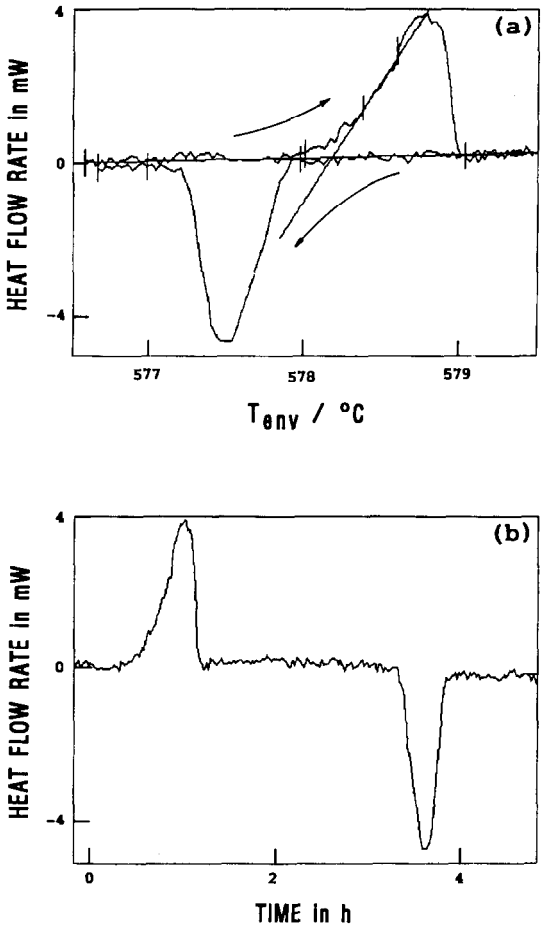

Fig. 6. Measured curves for the monoclinic to cubic and cubic to monoclinic transformations for sample 1 (Aldrich). (a) Heat flow rate vs. environment temperature; the arrows indicate increasing time. (b) Heat flow rate vs. time.

the inflection point of the curve $\phi(T_{env})$ and the baseline. It turned out (see Discussion below) that in the case of the transformation from cubic to monoclinic, no significant difference could be determined between T_i and T_e, so that only one of them is reported in Table 1, where the average values and corresponding standard deviations (of a single measurement with respect to the average) are given for the different samples.

The enthalpy changes for the transformation corresponding to some of these experiments (those experiments that included the complete transformation of the sample), were also determined by means of numerical integration of the area under the peaks as a function of time. The results for the three samples are given in Table 2.

The uncertainties given in the fourth column of Table 2, were calculated

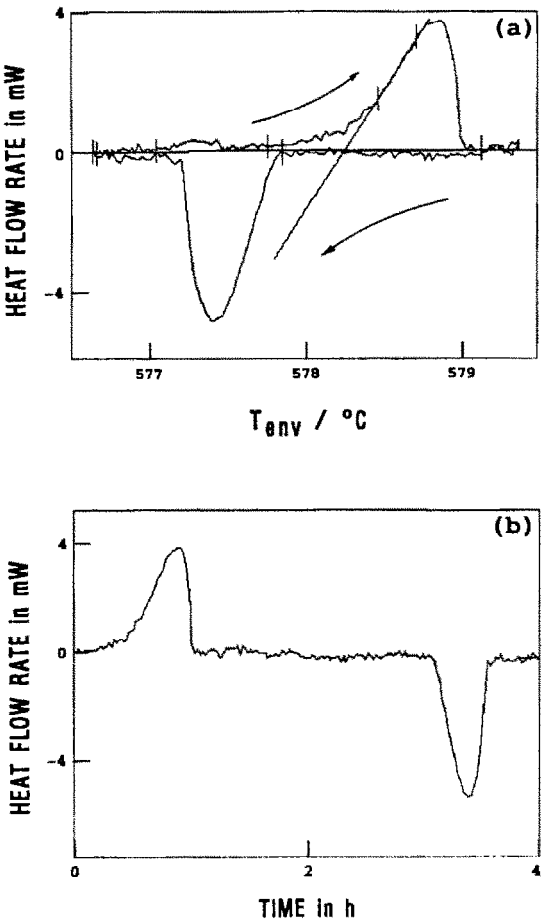

Fig. 7. Measured curves for the monoclinic to cubic and cubic to monoclinic transformations for sample 2 (Merck). (a) Heat flow rate vs. environment temperature; the arrows indicate increasing time. (b) Heat flow rate vs. time.

by adding in quadrature the uncertainties given in columns 2 and 3, and dividing by $\sqrt{2}$. The smaller uncertainties obtained for sample 3 are a direct consequence of an electronic improvement in furnace control that increased the signal to noise ratio of the experiments.

DISCUSSION

Calorimetric determinations of the phase-transition temperature and enthalpy change of the solid–solid phase transition of lithium sulfate have been made in the past by many authors. Hatem [13] presents one of the most recent determinations as well as a survey of previous ones, showing a

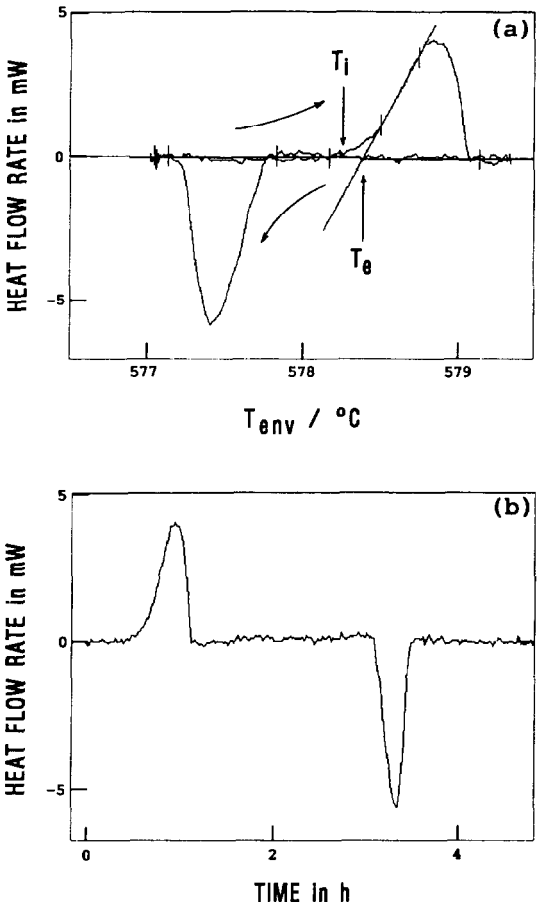

Fig. 8. Measured curves for the monoclinic to cubic and cubic to monoclinic transformations for sample 3 (Alfa). (a) Heat flow rate vs. environment temperature; the arrows indicate increasing time. (b) Heat flow rate vs. time.

TABLE 1

Onset temperature T_i and extrapolated temperature T_e of the solid–solid phase transition of Li_2SO_4 for the three powder-samples investigated [a]

Sample	Monoclinic to cubic		Cubic to monoclinic
	T_i/°C	T_e/°C	T_i/°C ≈ T_e/°C
1	577.82 ± 0.08(41)	578.17 ± 0.04(32)	577.90 ± 0.02(24)
2	577.98 ± 0.05(14)	578.28 ± 0.03(22)	577.84 ± 0.02(8)
3	578.30 ± 0.03(23)	578.38 ± 0.02(23)	577.78 ± 0.02(14)

[a] Each entry in the table represents the average value and standard deviation of a single measurement, that resulted from repeating the experiment the number of times indicated within parentheses. All the measurements correspond to average heating and cooling rates between 8 and 20 mK min^{-1}.

TABLE 2

Enthalpy changes for the monoclinic to cubic (and cubic to monoclinic) transformations of Li_2SO_4, for the three powder samples investigated [a]

Sample	ΔH/kJ mol^{-1}		$\lvert\Delta H\rvert$/kJ mol^{-1}
	Monoclinic to cubic	Cubic to monoclinic	Average
1	25.3 ± 0.9(10)	−25.9 ± 0.4(10)	25.60 ± 0.7
2	28.2 ± 0.9(12)	−27.9 ± 1.0(12)	28.05 ± 1.0
3	24.6 ± 0.5(15)	−24.9 ± 0.3(15)	24.75 ± 0.4

[a] Each entry in the table represents the average value and standard deviation of a single measurement, that resulted from repeating the experiment the number of times indicated within parentheses.

rather large scatter of values in the literature. As for the phase-transition temperature, even leaving out some values that differ noticeably from the others, those remaining range between 573 and 578°C, none of the authors claiming a much better accuracy than ±1°C. Most of those experiments have been made using thermocouples in order to measure temperatures, and heating rates of the order of several K min^{-1}. Under such conditions, and in the light of what has been discussed above regarding possible sources of error, a large scatter of results is to be expected.

A similar situation prevails for the enthalpy change of the transition, the corresponding values ranging between 21 and 29 kJ mol^{-1}. The presently reported results, given in column 4 of Table 2, that lead to an average value of 26.1 ± 1.7 kJ mol^{-1}, represent an improvement in this situation. However, no explanation can be given, for the time being, of the systematic difference repeatedly measured between sample 2 and the other two samples. For instance, molar surface-tension work due to the known expansion of lithium sulfate as it goes from the monoclinic into the cubic form [14], seems to be totally negligible. A value for it, smaller than 0.05 kJ mol^{-1}, is all that one gets, for any reasonable surface-tension value and for crystallites larger than 0.1 μm. Surface tension and crystallite size distributions, will be discussed below.

All that can be said in favor of the present enthalpy-change measurements is that the calorimeter is capable of an accuracy of ±3%, as already discussed above, and that for each sample the enthalpy changes for the direct and inverse transformation agree very well within this uncertainty limit.

Besides the fact that the results presented in Table 1 for the solid–solid phase-transition temperature of Li_2SO_4 represent at least a tenfold improvement in accuracy over previously known values, the high resolution of the calorimeter employed permits the observation of systematic

differences between the three samples that can be explained semiquantitatively. At the same time it will turn out to be clear that sample preparation (i.e. granulometry, dehydration process, etc.) is expected to play a significant role.

The explanation of those systematic differences is based on the change of phase-equilibrium temperature caused by interphase curvature (Gibbs–Thomson effect) [15] and the different size distribution of the crystallites that compose the powder samples. From the fact that the present measurements imply that smaller crystallites have a lower transition temperature, it will also be possible to conclude that interphase curvature is such that the monoclinic phase is on the concave side of the interphase.

In the utopian case of monoclinic-phase spherical particles of lithium sulfate of radius r, imbibed in a cubic-phase matrix of lithium sulfate, the phase-equilibrium temperature, $T(r)$, at constant pressure, is given by

$$T(r) = T_\infty \exp\left(\frac{V_m 2\gamma}{\Delta H r}\right) \tag{1}$$

where T_∞ is the phase transition temperature for $r \to \infty$, i.e. flat interphases and very large monocrystals, V_m is the molar volume of the spherical particles, γ is the surface tension between both phases, and $\Delta H < 0$, is the molar phase transition enthalpy from cubic to monoclinic.

Had we assumed instead cubic-phase spherical particles of radius r imbibed in a monoclinic-phase matrix, the sign of the exponent in eqn. (1) would have changed since $\Delta H > 0$ is in this case the molar phase transition enthalpy from monoclinic to cubic. Smaller crystallites would have had higher transition temperatures.

Equation (1) can be derived assuming thermodynamic equilibrium, by combining (1) the difference between the inner (inside the spherical crystallite) and outer pressures, i.e. $(2\gamma)/r$; (2) the condition that under a small change of r (due to growth of one of the phases at the expense of the other) the free energy of both phases should remain equal at equilibrium; (3) the well known expression for dP/dT given by the Clayperon–Claussius equation.

Setting aside the fact that it is hard to imagine the process associated with the first condensation or appearance of cubic-phase particles with radius r, in the midst of a monoclinic-phase crystallite (probably starting at the crystal defects that it might possess), and to assign a clear physical significance to r (perhaps a typical distance in the crystallite), an exact calculation of the temperature at which this is to occur would still require the knowledge of r, the surface tension γ, and the value of T_∞, none of which is available. We may still turn the problem around, for the sake of estimating typical values of r. We may postulate different values for T_∞ and γ, and solve eqn. (1) for r, thinking that the experimental values of T_i determined here (given in column 2 of Table 1) represent the temperature

TABLE 3

Values of r required in order to explain semi-quantitatively the observed onset temperatures, T_i (given in column 2 of Table 1 for each sample), based on eqn. (1), for $\gamma = 0.2\ J\ m^{-2}$ and several postulated values of T_∞

T_∞/°C	$r/\mu m$		
	Sample 1	Sample 2	Sample 3
578.4	1.2	1.6	6.7
578.5	0.99	1.3	3.4
578.6	0.86	1.1	2.2
578.7	0.77	0.94	1.7
578.8	0.69	0.82	1.3
578.9	0.62	0.73	1.1
579.0	0.57	0.66	0.96

at which the smallest crystallites of monoclinic phase begin to convert into the cubic phase. Table 3 represents the results of such a numerical venture, for several postulated values for T_∞ and for $\gamma = 0.2\ J\ m^{-2}$. The latter is a literature value [12] for the surface tension of liquid Li_2SO_4 in equilibrium with its vapor. Unfortunately, no value is available for the monoclinic/cubic γ value, but many solid salts in equilibrium with their vapor, present surface tension values ranging from $0.11\ J\ m^{-2}$ (KCl) to about $1.2\ J\ m^{-2}$ (MgO) [16]. Since in eqn. (1) surface tension and radius of curvature enter the combination γ/r, choosing a different value of γ changes the corresponding value of r (given in Table 3) in a proportional manner, i.e. reducing γ by a given factor, reduces r by the same factor. While experimenting with different values of γ, one might also consider that it is likely that the surface tension between the two solid forms of lithium sulfate is smaller than the surface tension between its liquid and vapor (used for Table 3), since the forces felt by an ion on the monoclinic/cubic interphase are perhaps better balanced.

The point of view that the measured temperature differences between samples are due to the Gibbs–Thomson effect is supported by the fact that the order of magnitude of the resulting values of r given in Table 3 coincides with the size of the randomly distributed product crystallites (0.2–1.0 μm) that have been observed during thermal dehydration of $Li_2SO_4 \cdot H_2O$ crystals [17].

Besides the dehydration process parameters, such as final pressure and temperature (held constant in the present study), the size-distribution of the product Li_2SO_4 crystallites may depend on the initial granulometry, heating and pumping speeds, as well as on the crystal defects (linear dislocations, etc.) which act as reactive sites for the dehydration reaction. This might therefore be the reason for the presently observed differences

between the three powder samples investigated. It is worth mentioning that a quantity of lithium sulfate corresponding to sample 1, was left to rehydrate completely over a period of several months (slowly, enclosed in the graphite capsule in normal air). After dehydrating it again, using the procedure described above, no differences were detected with respect to the results already given. This can be interpreted as an indication that the dehydration process used in the present work does not change the granulometry of the sample by a significant amount.

Further evidence about the influence that particle size might have on the transformation temperature, and on the shape of the measured curves, was gained by a series of transformation experiments starting with the sample completely in the monoclinic phase, and increasing T_{env} at a rate $\beta \approx 20\,mK\,min^{-1}$. After transforming only part of the sample from the monoclinic into the cubic form, the temperature T_{env} was decreased at an average rate $\beta \approx -10\,mK\,min^{-1}$. Surprisingly, so long as monoclinic material was still present, the transformation from the cubic into the monoclinic form started almost immediately, regardless of current value of T_{env}. This is evident from Fig. 9, representing a typical heat flow curve $\phi(T_{env})$ versus T_{env} of such an experiment, where the sharp decrease of ϕ, eventually attaining negative values, results from the heat release accompanying the cubic to monoclinic transformation. Needless to say that in each of these experiments the enthalpy change balance was verified by integration of ϕ(time) versus time, which also provided information about the proportion of material that had been converted from the monoclinic to the cubic form. In accordance with the arguments given above, an explanation of the curve shown in Fig. 9 can be based on the fact that at different values of T_{env}, different-sized crystallites comprising the sample, begin to transform from the monoclinic into the cubic form. As soon as T_{env} begins to decrease the particles that began transforming last (absorbing heat) begin to revert to the monoclinc phase, releasing the corresponding latent heat, and causing an abrupt decrease in ϕ. At lower values of T_{env}, correspondingly smaller crystallites begin to reconvert into the monoclinic phase. Moreover, the somewhat parabolic shape presented by the curves for lithium sulfate, in sharp contrast with the linear shapes observed for all the metals (see Fig. 5 for Zn), can also be understood with this model. At $T_{env} = T_i$ the smallest crystallites begin to transform. As T_{env} increases, larger, and still larger particles start transforming, adding to the slope of the continuously increasing $\phi(T_{env})$ curve, until the effect of the declining monoclinic population begins to take over. The slope will increase faster at temperatures corresponding to those sizes for which more crystallites are present in the sample. It is conceivable from this argument that the extrapolated temperature T_e, given in column 3 of Table 1, is representative of the transformation temperature corresponding to the average crystallite size in each sample (imagine for instance what would happen if only one

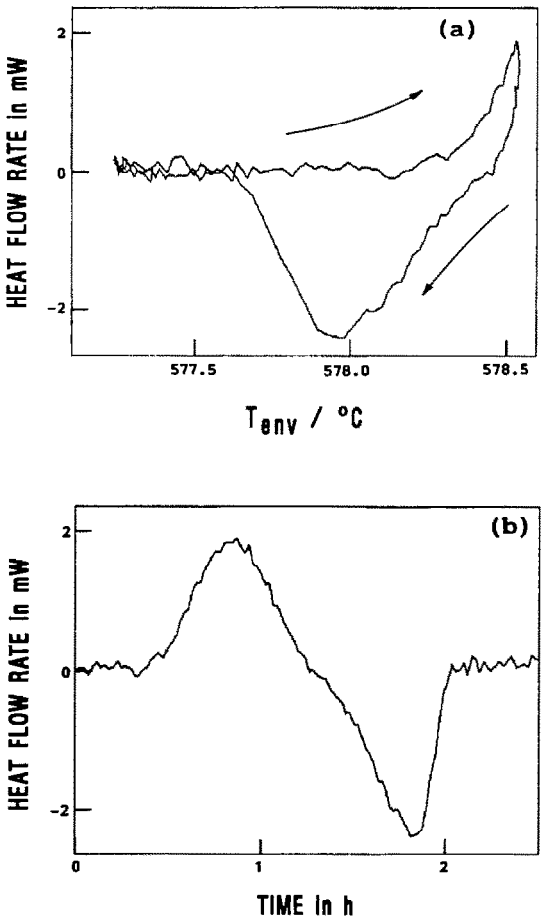

Fig. 9. Measured curves corresponding to the partial conversion (about 65%) of sample 3 from monoclinic to cubic followed by total reconversion to monoclinic. Notice that reconversion to monoclinic starts almost immediately, at a higher temperature than would have been expected. (a) Heat flow rate vs. environment temperature; the arrows indicate increasing time. (b) Heat flow rate vs. time.

size were present). Based on the same arguments, the steeper increase of $\phi(T_{env})$ observed for sample 3 as compared with sample 1, can also be interpreted as indicating a narrower crystallite size distribution in the former sample as compared with the latter. This also explains the differences in uncertainty with which T_i and T_e were determined for the different samples, since narrower crystallite-size distributions imply more sharply defined temperatures of transition.

In contrast to all that has been discussed so far for the monoclinic to cubic transformation, the reverse transformation seems to be controlled by the phenomenon of undercooling. This would explain the rather abrupt decrease of $\phi(T_{env})$ at $T_{env} = T_i$, and the consequent equality between T_i and

T_e. It may also be the reason for the smaller scatter of the corresponding T_i values for the three samples as compared to the scatter of T_i for the reverse transformation (see Table 1). Moreover T_i, assumed to be the undercooling temperature, decreases from sample 1 (the one with the smallest crystallites), to sample 2, to sample 3 (the one with the largest crystallites), as might be expected if a larger monocrystal were to have a lower undercooling temperature, as a result of a smaller surface to volume ratio, and if surface imperfections were to act as nucelation sites.

Additional experimental evidence for the undercooling hypothesis, is the fact that out of about 48 experiments converting the sample into the monoclinic phase, but starting with the sample completely in the cubic phase, on two occasions the measured value of T_i was below the average

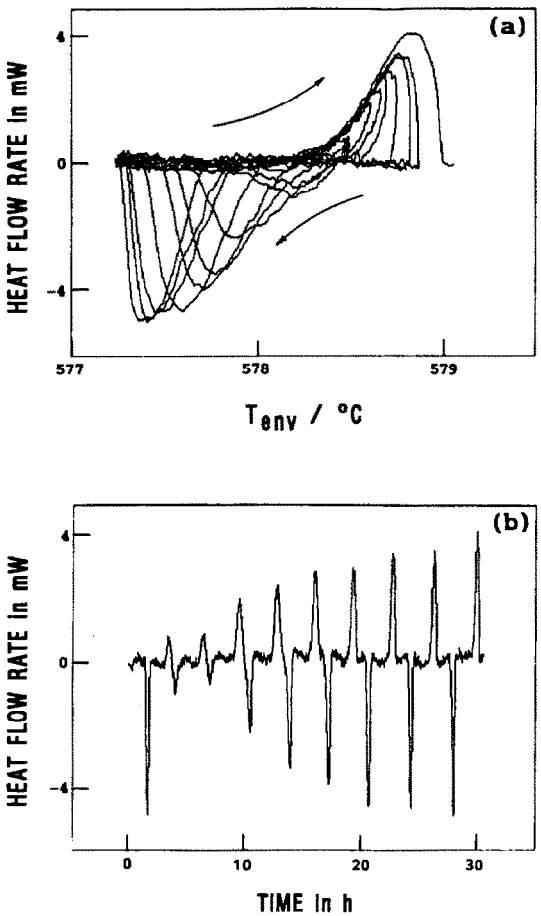

Fig. 10. Automatic run of nine consecutive cycles, converting each time a larger fraction of the sample from the monoclinic phase into the cubic phase followed by total reconversion to monoclinic. (a) Heat flow rate vs. environment temperature; the arrows indicate increasing time. (b) Heat flow rate vs. time.

value by about 0.15°C (seven times larger than the standard deviation!). This could be interpreted as an occurrence of unusually strong undercooling. In both cases, this happened after waiting for a relatively long time at the higher temperature end (several hours, whilst preparing the equipment in order to run an automatic set of conversions and reconversions). Possibly relaxation times are such that even a smaller than usual amount of material, that may provide nucleation sites, survives in a quasi-monoclinic phase if one does not wait long enough. Furthermore, many experiments related to those pictured in Fig. 9, showed that because of the availability of nucleation sites, so long as monoclinic phase is still present, conversion from cubic into monoclinic takes place at temperatures well above the measured undercooling temperatures. Figure 10, corresponding to sample 3, although slightly confusing because of the superposition of nine

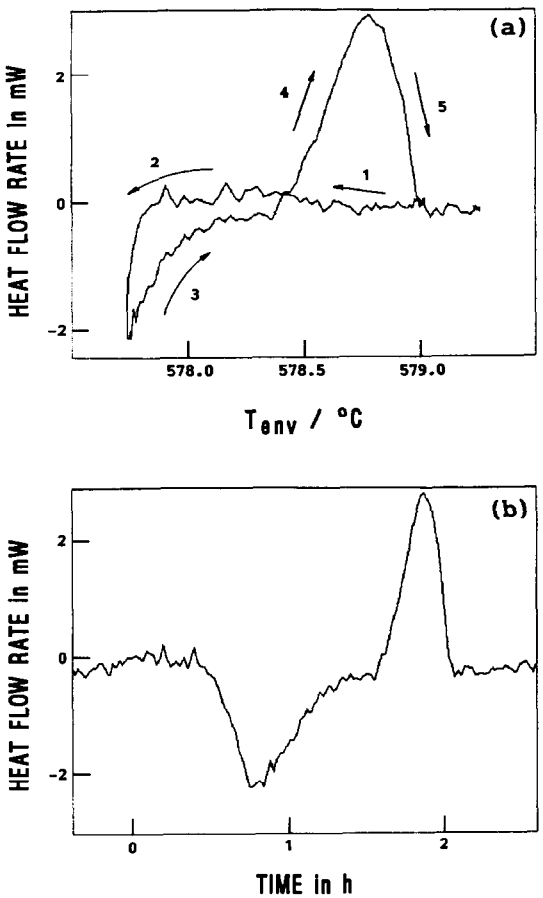

Fig. 11. Measured curves corresponding to the partial conversion (about 60%) of sample 3 from cubic to monoclinic followed by total reconversion to cubic. Notice that reconversion to cubic starts at the expected temperature. (a) Heat flow rate vs. environment temperature, the arrows indicate increasing time. (b) Heat flow rate vs. time.

consecutive cycles, converting a larger amount of sample from the monoclinc phase into the cubic phase each time, up to 100% conversion, illustrates this point. Some of the interesting shapes that can be observed in Fig. 10, may also be qualitatively explained with arguments based on crystallite size distribution, relaxation times and surviving nucleation sites. Looking at the overall envelope of the cubic to monoclinic transformations in Fig. 10 (negative heat flow rates), it is tempting to think about an extrapolated temperature T_e that would coincide with the value of T_e corresponding to the monoclinic to cubic transformation. Similar curves and behavior were observed for the other two samples.

Experiments such as those referred to in Figs. 9 and 10, were also run starting with each of the samples completely in the cubic phase, and decreasing T_{env} at a rate $\beta \approx 20\,\text{mK min}^{-1}$ (Fig. 11). After transforming only part of the sample from the cubic into the monoclinic form, the temperature T_{env} was increased at an average rate $\beta \approx 10\,\text{mK min}^{-1}$. As might be expected from the model developed so far, and unlike the observations made and described above for the reverse transformation, no material started to reconvert into the cubic phase until the corresponding temperature T_i was reached, despite the presence of particles in the cubic phase.

CONCLUSIONS

Employing a high-accuracy heat-flow calorimeter in order to study the phase transformations between the two solid forms of Li_2SO_4 it is possible to draw the following conclusions:

(a) The enthalpy change between the two high temperature forms of solid lithium sulfate resulted in $\Delta H = 26.1 \pm 1.7\,\text{kJ mol}^{-1}$. The relatively large uncertainty (twice as large as expected) is due to as yet unexplained differences between the three powder samples investigated (see Table 2).

(b) The temperature of transformation has been determined for each of three powder samples, with at least a tenfold improvement in accuracy over previously known values. Once the dehydration procedure ($P = 0.3\,\text{Pa}$, $t = 150°\text{C}$, several hours) is applied to a given sample, the transformation from one phase into the other may be reversed and repeated without any detectable change in the transformation temperature. The same happens if the sample is allowed to hydrate slowly and is dehydrated again with the same procedure. However, the transformation temperature is sample dependent. The origin of the differences can be explained semi-quantitatively by means of the Gibbs–Thomson effect, in terms of the size distribution of the crystallites that compose the sample, which should depend on its initial granulometry and the dehydration procedure used.

The onset temperatures for the monoclinic to cubic transformation, for sample 1 (Aldrich), sample 2 (Merck) and sample 3 (Alfa), are 577.82 ± 0.08, 577.98 ± 0.05 and $578.30 \pm 0.03°\text{C}$, respectively. They are

believed to represent the transformation temperature of the smallest crystallites present in the sample. Extrapolated temperatures, representative of the transformation temperature corresponding to the average crystallite size in samples 1, 2 and 3, are 578.17 ± 0.04, 578.28 ± 0.03 and 578.38 ± 0.02°C, respectively. For the cubic to monoclinic transformation, the corresponding onset temperatures for the same three samples are 577.90 ± 0.02, 577.84 ± 0.02 and 577.78 ± 0.02. These are believed to represent the end temperatures of undercooling, just as nucleation of the new phase begins.

(c) At equilibrium, interphase curvature is such that the monoclinic phase is on the concave side of the interphase.

ACKNOWLEDGMENTS

This work was performed in the framework of a Technical Cooperation Agreement between the Republic of Argentina and the Federal Republic of Germany, under the auspices of the Bundesministerium für Wirtschaftliche Zusammenarbeit. Thanks are due to Dipl.-Volkswirt H. Apel (PTB) and Dr. D. Schlipf (GTZ) for their efficient administrative support, and to Dr. S.M. Sarge for helpful discussions and for supplying the samples. The author is very grateful to Lic. P. Giorgio for help in developing the computer software that controls the experiments, and to Dr. C. Puglisi for the microscopy work. Thanks are also due to Lic. M. Jimenez Rebagliati, Ing. C. T. Lewis, Lic. L. Menendez, and Lic. G. A. Rangugni, for their effective collaboration.

REFERENCES

1 M. Tischler and M. Koremblit, in J.F. Schooley (Ed.), Temperature, Its Measurement and Control in Science and Industry, American Institute of Physics, New York, 1982, pp. 383–390.
2 M. Tischler and C. Anteneodo, Proc. Int. Symp. Temperature Measurement in Industry and Science, China Academic Publishers, Beijing, 1986, pp. 192–197.
3 M. Tischler and W. Neubert, in J.F. Schooley (Ed.), Temperature, Its Measurement and Control in Science and Industry, American Institute of Physics, New York, 1992, pp. 1049–1060.
4 A. Kvist and A. Lundén, Z. Naturforsch., Teil A, 20 (1965) 235–238.
5 L. Nilsson, J.O. Thomas and B.C. Tofield, J. Phys. C: Solid State Phys., 13 (1980) 6441–6451.
6 K. Schroeder and C.A. Sjoblom, High Temp.-High Pressures, 12 (1980) 327.
7 H.K. Cammenga, W. Eysel, E. Gmelin, W. Hemminger, G.W.H. Höhne, S.M. Sarge, PTB-Mitt., 102 (1992) 13.
8 R. Kabert, L. Nilsson, N.H. Andersen, A. Lundén, J.O. Thomas, J. Phys.: Condens. Matter, 4 (1992) 1925–1933.
9 E.A. Secco, J. Solid State Chem., 96 (1992) 366–375.
10 H. Preston-Thomas, Metrologia, 27 (1990) 3–10.
11 C.A. Busse, J.P. Labrande and C. Bassani, Temperature Measurement 1975, Inst. Phys. Conf. Ser., 26 (1975) 428.

12 Eric A. Brandes (Ed.), Smithells Metals Reference Book, 6th edn., Butterworth, London, 1983.
13 G. Hatem, Thermochim. Acta, 8 (1985) 433–441.
14 B.E. Mellander and L. Nilsson, Z. Naturforsch., Teil A, 38 (1983) 1396–1399.
15 W. Thomson, Proc. R. Soc. Edinburgh, 7 (1870) 63.
16 G.C. Benson and R.S. Yuen, in E.A. Flood (Ed.), The Solid–Gas Interface, Marcel Dekker, New York, 1967.
17 H. Tanaka, N. Koga and J. Šesták, Thermochim. Acta, 203 (1992) 203–220.